Conjugate heat transfer analysis in high speed flows

M.S.R. Chandra Murthy, P. B. Manna and Debasis Chakraborty

Proceedings of the Institution of Mechanical Engineers, Part G: Journal of Aerospace Engineering published online 27 March 2013
DOI: 10.1177/0954410012464920

Original Article

Institution of MECHANICAL ENGINEERS

Journal of AEROSPACE ENGINEERING

Proc IMechE Part G:
J Aerospace Engineering
0(0) 1–10

DOI: 10.1177/0954410012464920
uk.sagepub.com/jaero

SAGE

Conjugate heat transfer analysis in high speed flows

MSR Chandra Murty, P Manna and Debasis Chakraborty

Abstract

Conjugate heat transfer studies are presented for high speed aerospace vehicle using commercial CFD software. Navier Stokes equations in the fluid domain and transient heat conduction equations in the solid domain are solved simultaneously to obtain the skin temperature history and other flow parameters. The computational methodology is applied to predict the surface temperature of high speed aerospace vehicle after validating the methodology against experimental results. Validation cases include laminar flow past axisymmetric double cone at Mach 4.57 and turbulent flow past circular cylinder at Mach 6.7. Computed flow field including cold wall heat flux, surface temperature distribution, surface temperature history match nicely with experimental as well as other numerical results. Temperature dependent material properties are found to have significant effect on the surface temperature prediction. Computed surface temperature of a high speed aerospace vehicle show good overall match with flight measured values.

Keywords

Conjugate heat transfer, high speed flow, heat flux

Date received: 1 June 2012; accepted: 25 September 2012

Introduction

High speed aerospace vehicles (rockets and missiles) experience adverse thermal environment during its ascent phase due to aerodynamic heating. The severity of aerodynamic heating depends on flight trajectory, vehicle geometry and flow condition. The higher is the flight speed, the higher is the aerodynamic heating. Aerothermal effects are important for fluid flow as well as for the heat conduction in the structure; especially for structures with low rigidity. The deformation due to aerodynamic load and aerothermal effect could alter the flow and heat transfer process significantly[1] The material choice and wall thickness are largely dependent on the accurate estimation of temperature distribution of the vehicle structure. So, for the prediction of aerodynamic load and aero thermal effect of high speed vehicle, it is necessary to consider the fluid flow and heat conduction to the structure simultaneously. In the past, the problem was simplified by calculating first the aerodynamic field and then evaluating the temperature inside the solid body separately by imposing a prescribed wall heat flux or temperature at the interface. Thus, the complexity of heat transfer processes between the fluid and the vehicle structure is described by a predetermined heat transfer coefficient which shows that the heat transfer process is independent of the solid properties. With the advent of powerful computer and robust numerical algorithms, it is possible to solve the fluid flow equations and the energy equation in the solid simultaneously to address the coupling of heat transfer at a solid/fluid interface which is known as conjugate heat transfer (CHT) in the literature.

Due to the importance and vast application of CHT problems in kinetic heating, turbo-machinery, reentry vehicles, laser irradiation applications, heating ducts etc, researchers showed an increasing interest in this research area over the last ten to fifteen years. Manna and Chakraborty[2] simulated low speed CHT problems for laminar flow over a flat plate and turbulent flow between two parallel plates using commercial software and obtained good match between the computed and experimental temperature and heat transfer coefficient values. Marineau et al.[3] verified and validated the CHT capability of the GASP code[4] for both low speed and high speed boundary layers ($M_e = 0.089$–2.3, M_e is the Mach number at the edge of the boundary layer) and obtained good agreement with experimental values of surface temperature and Stanton number. The authors also

Defence Research & Development Laboratory, Hyderabad, India

Corresponding author:
Debasis Chakraborty, Directorate of Computational Dynamics, Defence Research & Development Laboratory, P.O. Kanchanbagh, Hyderabad, India Tel: +91-40-24583310, Fax: +91-40-24340037.
Email: debasis_cfd@drdl.drdo.in

compared the computed flow field and the wall temperature distribution with experimental data of an axisymmetric supersonic nozzle involving heated flow of air and a water cooled wall. Hassan et al.[5] presented an iterative loose coupling between a Finite Volume CFD code and a Finite Element material thermal response code and used it to study ablation phenomena on a reentry vehicle flying along a ballistic trajectory. Shope[6] developed a CHT method to predict the flow field of a water-cooled nozzle for several coolant flow conditions in a high-enthalpy wind tunnel at Arnold Engineering Development Centre (AEDC). The developed method involved (1) space marching Euler method, (2) 1-D heat conduction equation and (3) an empirical treatment of the convective heat transfer due to flow boiling. The theoretical water coolant temperature rise was shown to agree quite well with the experiment. Engblom et al.[7] also validated the same experimental results with a 3-D Reynolds Averaged Navier Stokes (RANS) solver, a 3-D solid body heat conduction model, and an empirically-based 1-D upwind coolant solver. The CHT capabilities of Wind-US[8] code for different hypersonic applications are presented in Ref. 9–11.

Ferrero and D'Ambrosio[12] compared wall temperature distribution and temperature history of CHT analysis with the wind tunnel test results of axisymmetric double cones made of UHTC (Ultra High Temperature Ceramic material) for Mach 4.57 at DLR Koeln, Germany. A second order spatial and temporal Essentially Non Oscillatory (ENO)[13] based explicit finite volume flow solver was coupled with finite volume based heat conduction equation. The computed numerical results showed fairly good agreement with available experimental results. Dechaumphai et al.[14,15] demonstrated an excellent comparison between an integrated fluid-thermal-structural analysis with the experimental surface pressure and heat transfer results[16] (performed in the NASA Langley 8-foot High Temperature Tunnel) of Mach 6.47 flow over a 3 inch diameter and 0.5 inch thick, stainless steel cylinder. The solution of the Navier-Stokes equations for predicting aerodynamic heating and the solution of the Taylor-Galerkin algorithm for the associated thermal-structural equations are coupled in one integrated computer program. Zhao et al.[17] reported a very good comparison of computed surface pressure, cold wall heat flux, hot wall heat flux and temperature distribution with experimental results.[16] The integrated aerothermal analysis included commercial RANS solver,[18] solution of thermal heat conduction equation and a finite-element based quasi-static structural analysis.

Although few studies are reported in the literature regarding temperature prediction through CHT analysis for high speed canonical problems, the estimation of temperature in complete flight trajectory for high speed aerospace vehicle is very limited. Accurate estimation of surface temperature is very important to determine choice of material and material thickness. In the present work, we estimated the skin temperature of high speed aerospace vehicle through conjugate heat transfer analysis using commercial software Fluent.[19] A FFTB method (Flux Forward, Temperature Backward) is used for exchange of heat flux and temperature between the solid and fluid domain within the inner loop of time step. The computational methodology is first validated against the wind tunnel test results for (1) laminar flow over axisymmetric double cone at Mach 4.57[12] and (2) turbulent flow over circular cylinder at Mach 6.47[16] and the computed surface pressure, surface temperature, heat flux and temperature distribution are compared with experimental and other numerical results. The effect of temperature dependent material properties on the surface temperature is investigated. The validated methodology was then applied to predict the surface temperature of a high speed aerospace vehicle and computed surface temperature history is compared with flight measured values.

Methodology

The computational domain of the CHT problem consists of the fluid domain and solid domain. Three dimensional RANS equations are solved for velocity components, pressure, density and temperature in the fluid domain and the energy equation is solved for temperature in the solid domain. The fluid energy and the solid energy equations are coupled for the identical conditions of temperature and heat flux at the solid–fluid interface. In Fluent, the fluid flow equations are solved by employing a cell-centered finite volume method based on the linear reconstruction scheme that allows use of computational elements with arbitrary polyhedral topology, including quadrilateral, hexahedral, triangular, tetrahedral, pyramidal, prismatic and hybrid meshes. A density based implicit coupled solver is chosen for solving the governing equations of continuity, momentum and energy simultaneously. The Advection Upstream Splitting Method ($AUSM^{+}$)[20] is used for spatial discretization of the inviscid fluxes, whereas diffusion terms are discretized by a second order central differencing scheme. Temporal terms are also discretized through a second order scheme. The discretized algebraic equations are solved using a point-implicit linear equation solver (ILU factorization scheme on a symmetric block Gauss-Seidel) in conjunction with an algebraic multi-grid (AMG) method to accelerate solution convergence. Both laminar and turbulent cases are solved depending on the Reynolds numbers encountered in different simulations. Different turbulence and transition models namely, Menter's SST model[21] and 4 equations transition model[22] are employed. Since the test medium contained different species like O_2 and O, transport equations for these

species are also solved alongwith the Navier Stokes equations.

Gas–solid interface boundary condition

In general, at the gas –solid and solid –solid interface for CHT approach, the energy balance is done using FFTB method (Flux Forward, Temperature Backward). At the interface of two different regions the heat flux ($k\frac{\partial T}{\partial n}$) and the temperature ($T$) must be balanced.

$$T_1|_{\partial_{1-2}} = T_2|_{\partial_{2-1}} \tag{1}$$

$$k_1 \left.\frac{\partial T_1}{\partial n}\right|_{\partial_{1-2}} = k_2 \left.\frac{\partial T_2}{\partial n}\right|_{\partial_{2-1}} \tag{2}$$

(Suffix 1 and 2 refer to fluid and solid zones respectively).

The boundary heat flux at the common interface in the second domain is prescribed equal to the calculated heat flux in the first domain (Flux Forward). With this Neumann boundary condition, the temperature distribution on the second domain can be computed. The temperature profile obtained in the second domain at the common interface is prescribed back to the first domain as a Dirichlet boundary condition (Temperature Back). The temperature distribution and the heat flux are then computed in the first domain and the loop is iterated till the temperature and heat flux differences at the domain interface are below the desired numerical error. When the convergence is reached the physical time step is incremented and iteration for the next time step starts. The time step for the numerical simulation is calculated based on method that the thermal pulse within the solid materials should not cross more than one computational cell within a prescribed time step. This is calculated as follows,

$$\delta t = \frac{\delta x^2}{2\alpha} \tag{3}$$

where δt is the time step, δx is the smallest cell characteristic length in the solid domain and α is thermal diffusivity of the solid materials.

Validation studies

The computational methodology has been validated against two experimental results of high speed flows (1) Laminar flow past axisymmetric double cone at Mach 4.75[12] and (2) Turbulent Flow past circular cylinder at Mach 6.45.[16] Brief description the experimental geometry, material properties and flow conditions, important flow features of these experiments are presented in the next subsections.

Laminar flow past axi-symmetric double cone at Mach 4.75

Description of the experiment. An axisymmetric double cone made of Ultra High Temperature Ceramic (UTHC) (also known as ziroconium diborade (ZrB_2)) was tested at Mach 4.75 in the L2K high temperature tunnel at DLR Koeln in Germany. It was supported with a copper made structure fixed to a bench. The schematic of the geometry is shown in Figure 1. The time history of surface temperature was measured by an infrared camera and also by a pyrometer. General details of experimental test calibration and measurement analysis has been reported in Ref. [23]. The free stream Mach number, pressure and temperature were 4.57, 272 Pa and 740 K, respectively. A mixture of nitrogen and oxygen was used as test medium and the mass fraction of various species Y_{N2}, Y_{O2}, Y_O are 0.793,0.113, 0.092 respectively. The free stream Reynolds number calculated based on the flow parameters is 2313 and hence laminar calculations are carried out. Thermal conductivity (W/(m-K), density (kg/m^3),C_p (J/Kg-K)) of UHTC and oxygen free copper are 66, 6000, 628 and 387.6, 8978 and 381, respectively. Wall temperature history at 4 mm and 35 mm from the nose was measured for 90 sec duration using infrared camera.

Results and discussion

A very fine structured grid is generated around the body containing 144 points in the longitudinal (X) and 160 points in radial direction (Y) as shown in Figure 2. The grid is very fine near the boundary layer. The grid independence of the solution is demonstrated by comparing the wall temperature history with two different grids. Since, the vitiated air stream contains O_2 and O species, transport equations for these two species are also solved alongwith the Navier Stokes equations. A time step of 1 ms is considered for the present calculation. The temperature distributions in the symmetry plane at 30 and 60 s are compared in Figure 3. The bow shock, the separation shock, reattachment shock, the separated flow region are clearly visible in the figure. Following Edney,[24] the shock–boundary layer interaction type can be classified as Type V, where the intersection of bow shock and the impingement shock from the same family forms a supersonic jet instead of simple shear layer. Temporal evolution of separation bubble in the double cone corner is depicted in velocity vector plot (Figure 4). The size of the separation zone is seen to increase up to 40 s, and remains constant thereafter.

The computed temperature histories at 4 and 35 mm from the nose cone are compared with the experimental values in Figure 5(a) and (b) respectively. The computed temperature history at $X = 4$ mm with coarse grid (120×120) is also shown

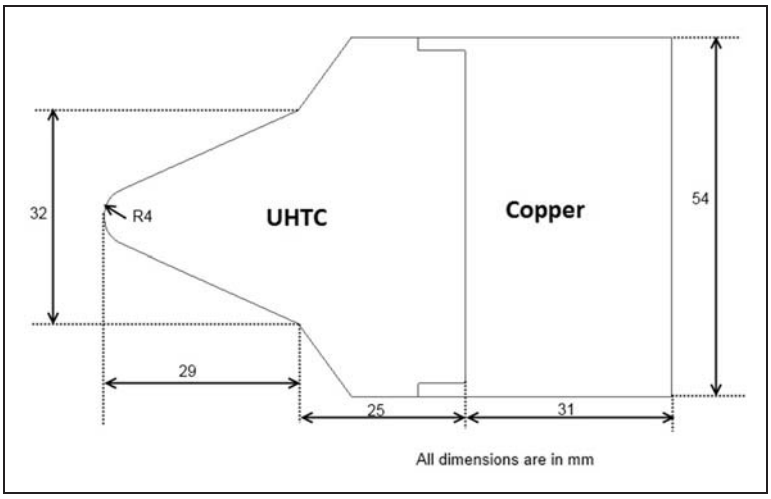

Figure 1. The schematic of double cone geometry[12] for which the simulation is carried out.

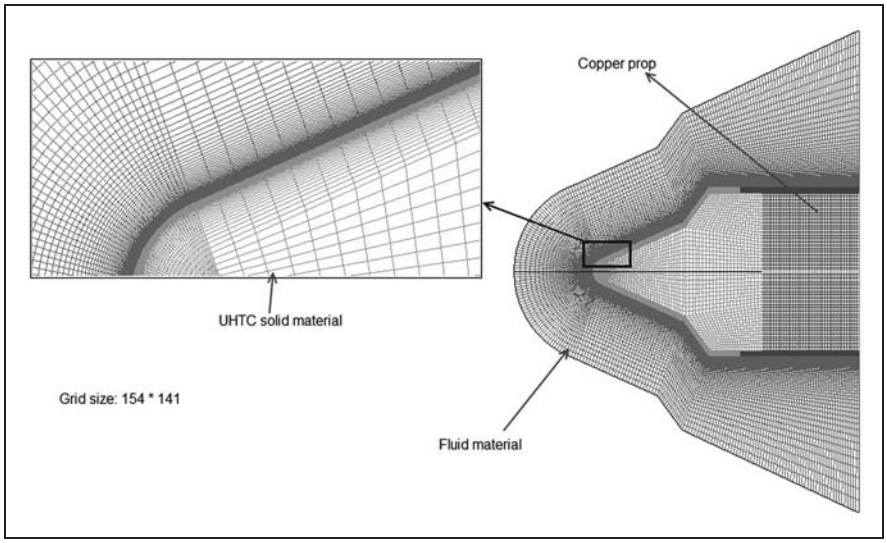

Figure 2. Grid distribution around the configuration (a) Complete body (b) around the nose cone.

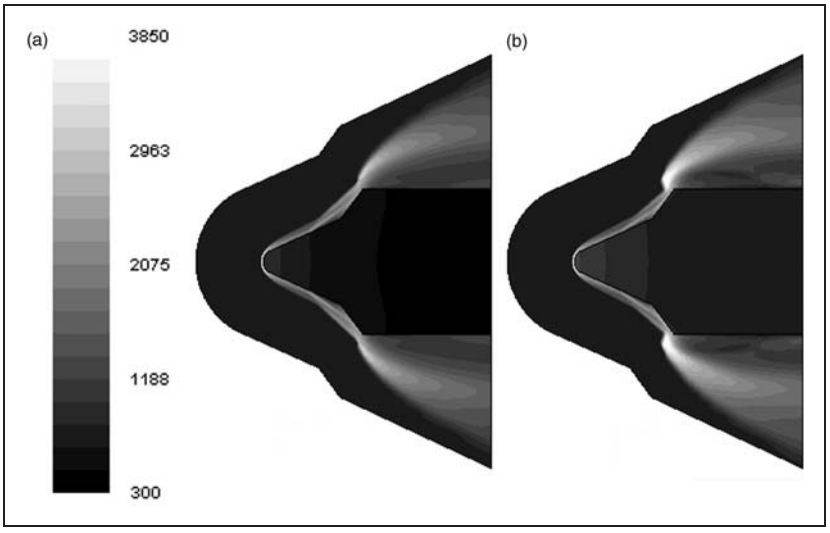

Figure 3. Temperature (K) distribution in the symmetry plane (a) 30 s (b) 90 s.

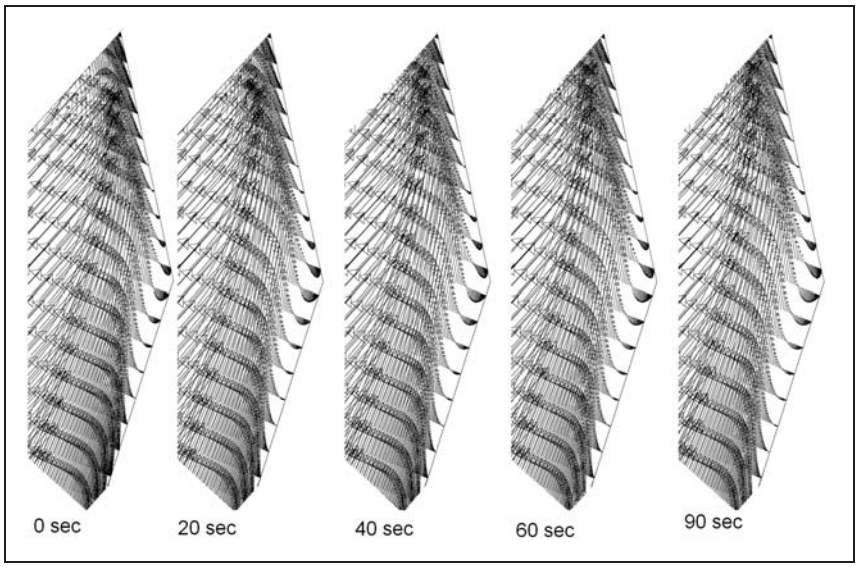

Figure 4. Velocity vector in the separation zone with increasing time.

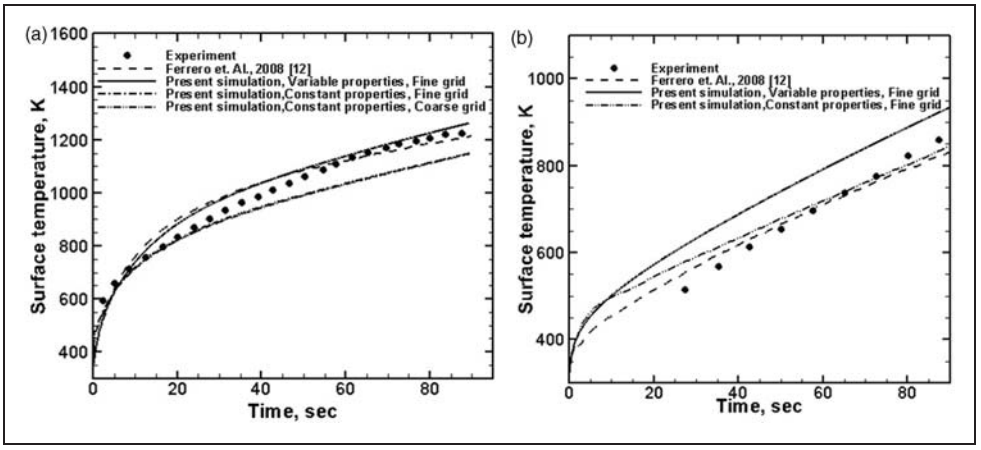

Figure 5. Comparison of computed and measured temperature history at (a) $X = 4$ mm (b) 35 mm.

in the figure to demonstrate the grid independence of the solution. Temperature dependent material properties viz., density and thermal conductivity and specific heat of UHTC are taken from Ref. 25 and 26 respectively whereas; temperature dependent material properties of copper are taken from Ref. 27. Computations with variable thermo-physical properties of the surface materials match better with the experimental results; while the computation with the constant material property underpredict the surface temperature. The maximum deviation of computed surface temperature from the experimental value is within 2% at the longitudinal location (X) 4 mm. The CHT prediction of Ferrero and D'Ambrosio[12] matches well with the experimental results but at later time ($t > 60$ s), the present computation with temperature varied material properties agrees better with the experimental values. At 35 mm location, the calculation with constant material properties matches better with the experimental data compared to the values obtained from temperature dependent material properties calculation. A parallel upward shift is seen in the prediction with variable thermal properties compared to experimental data.

The axial distribution of the surface temperature at 60 s is compared in Figure 6 with experimental and other numerical data.[12] The computed surface temperatures with temperature dependent material properties agree with the experimental data in the forward portion; while the computed values with constant material properties match better with experimental data in rearward portion. The surface temperature predicted by Ferrero et al.[12] lies in between the present computation with constant and variable material properties. The reason for this anomaly is not known.

Turbulent flow past circular cylinder at Mach 6.45

In the second validation case, the aerothermal flow field over a circular cylinder at Mach 6.45 is compared with experimental and other numerical results.

Description of the experimental condition[16] for which is the simulation is carried out

A 76.2 mm diameter, 12.7 mm thick, 610 mm long cylinder made of 321 stainless steel is tested at Mach 6.47 in the NASA 8-Foot high temperature hypersonic blow down tunnel. Methane and air is burned in a high-pressure combustor in this facility to obtain the high energy test gas. The schematic of the experimental set up is shown in Figure 7. The Mach number, pressure, temperature and Reynolds number of the gas flow at the test section are 6.47, 648 Pa, 241.5 K and 1.312×10^6 per meter respectively. Approximately 50 low frequency strain-gage type pressure transducers and chromel-constantan (Type E) and chromel-alumel (Type K) coaxial thermocouples were placed at several longitudinal circumferential locations along the cylinder surface to accurately determine the aerodynamic pressure and heating rate distribution. Details of the experimental configurations, the tunnel flow conditions, and the experimental results are given in Ref. 16.

Results and discussion

Taking the advantage of the symmetry, only one-half model is simulated. Very fine structured grid involving 140 grid points in the axial direction and 110 grid points in the radial direction is employed in this case. To predict the heating rate accurately, the wall boundary layer is resolved with a very fine mesh of minimum grid spacing of 1 μm, which corresponds to y^+ of 0.2. A very fine mesh (140×20) is also taken in the solid region of the cylinder. Similar to the first validation case, 1 ms time step is also employed in the simulation. As the Reynolds number in the test section is 1.312×10^6/m, transitional simulation is performed by employing Menter's 4 equations transition model.[22] The qualitative feature of the flow field is presented in the composite plot in Figure 8 where the Mach number, pressure and temperature distributions at 5 s are presented in the cross-sectional plane. The numerically generated schlieren picture is compared with measured schlieren in Figure 9. We can observe a very good agreement of the shock locations

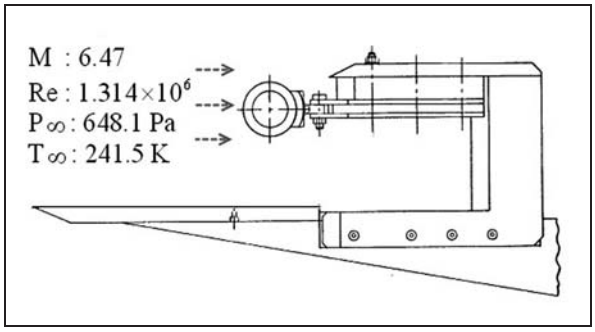

Figure 7. Schematic of experimental set up[16] for which the simulations are carried out.

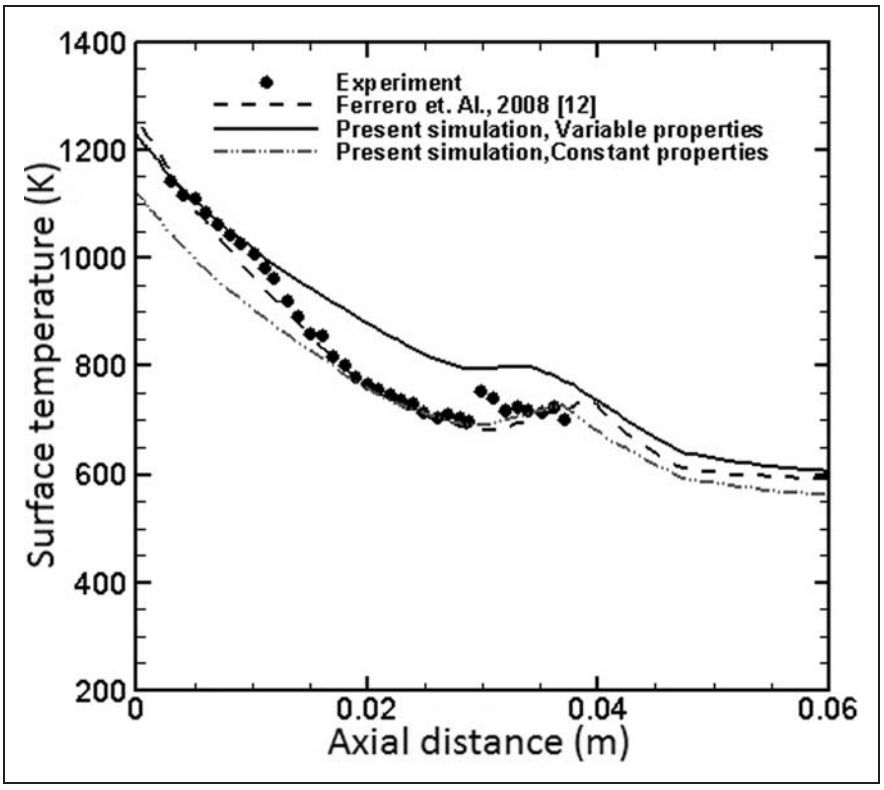

Figure 6. Comparison of axial distribution of surface temperature at 60 s.

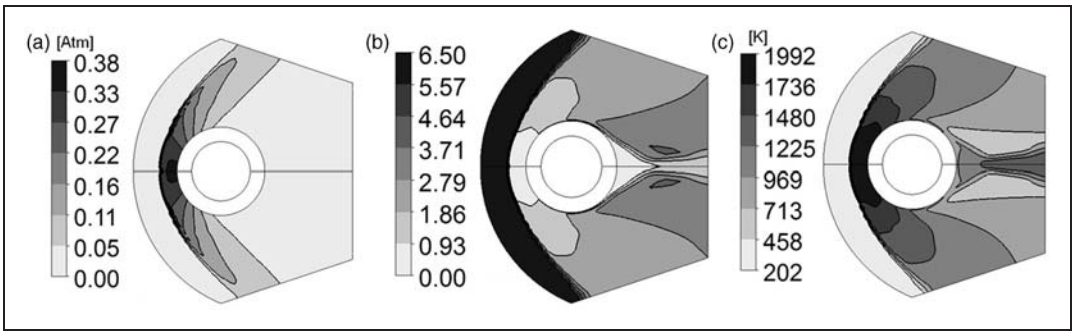

Figure 8. Flow field distribution at 5 s (a) Pressure (atm) (b) Mach number (c) Temperature (K).

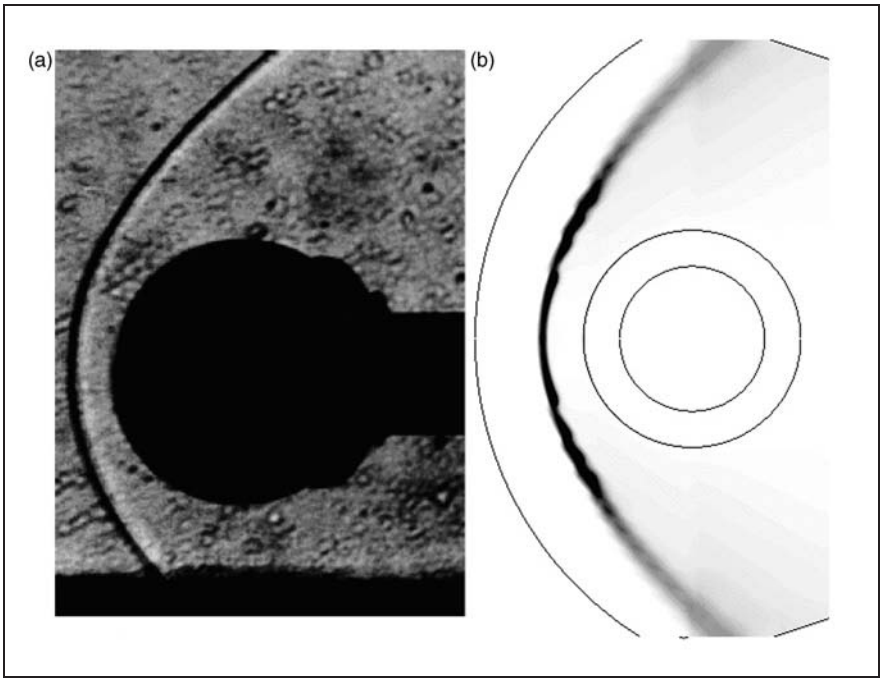

Figure 9. (a) Experimental and (b) numerical schlieren picture in the symmetry plane.

between the two. The predicted pressure and temperature behind the shock wave (pressure 33 kPa and temperature 2000 K) are in good agreement with other calculation reported in the literature[15,17] indicating that overall flow features are well captured. The circumferential variation of surface pressure is compared with experimental values and the computations of Dechaumphai et al.[15] and Zhao et al.[17] in Figure 10 and the computed surface pressures match well with the experimental values. The computed cold wall heat flux and surface temperature are compared with the experimental and other numerical results[17] in Figure11(a) and (b), respectively. As we proceed away from the stagnation point, the heat flux is reducing monotonically. The variation of experimental

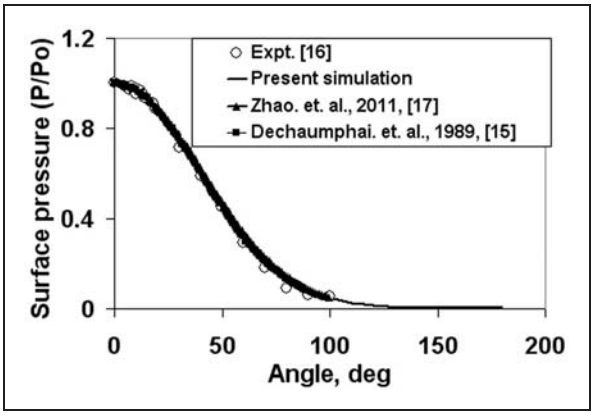

Figure 10. Variation of circumferential surface pressure.

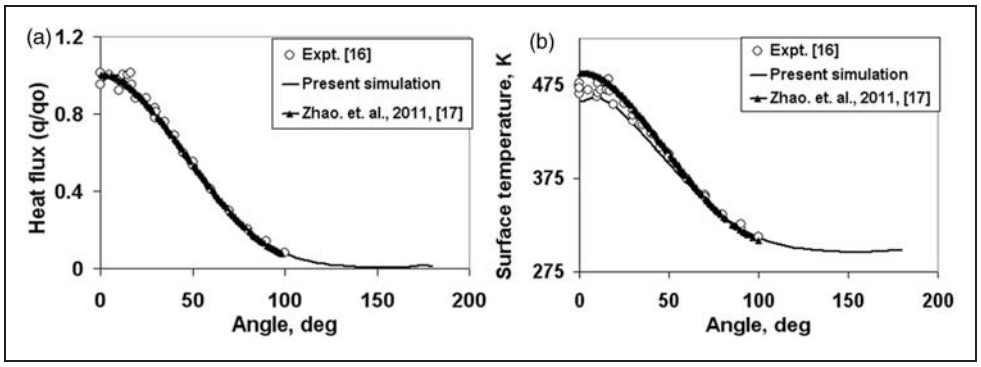

Figure 11. Comparison of circumferential variation (a) cold wall heat flux (b) surface temperature.

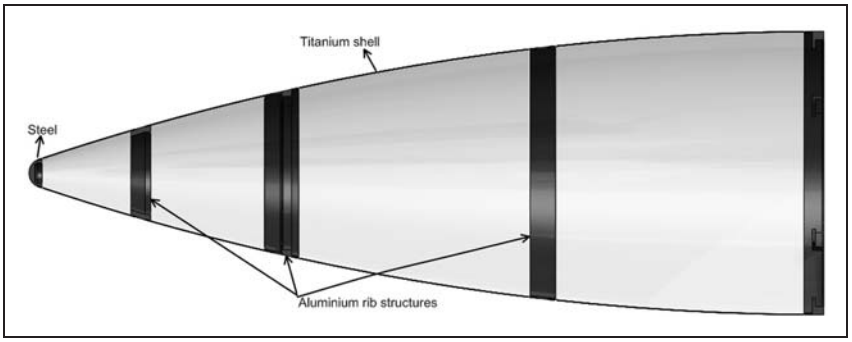

Figure 12. Schematic of high speed flight vehicle geometry.

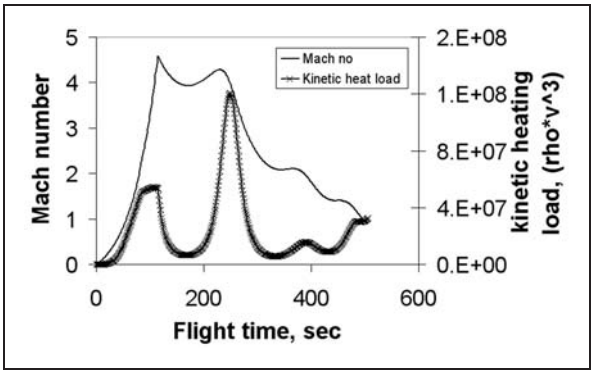

Figure 13. Mach number and kinetic heat load history of the flight vehicle.

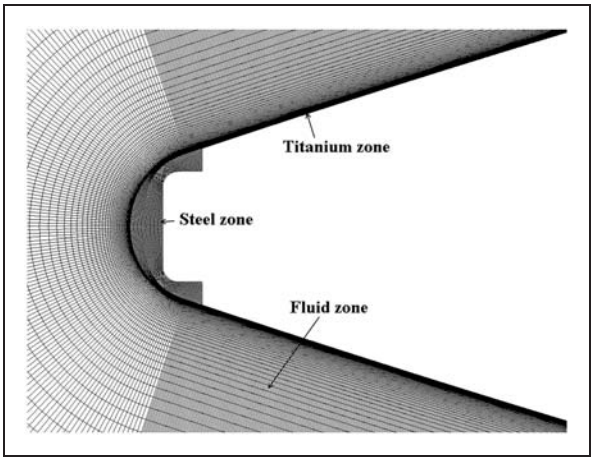

Figure 14. Computational mesh in the forebody.

heat flux in the region $10^\circ < \theta < 25^\circ$ is not observed in the computed values. A very good agreement is obtained between the present computation with the experimental results for both cold wall heat flux and temperature; while the computation of Zhao et al.[17] showed higher surface temperature in the region $10^\circ < \theta < 25^\circ$.

Application of CHT analysis of high speed aerospace vehicle

Viscous flow kinetic heating analysis of a flight vehicle is performed using Conjugate Heat Transfer (CHT) methodology. The schematic of the forebody of the flight vehicle is shown in Figure 12. The vehicle's shell structure is made of 1.5 mm thick titanium and the nose cone portion is made of 20 mm thick AISI-304 stainless steel to counter stagnation point heating. Different titanium shell sections are joined together with aluminum ribbed structural elements. To ensure proper thermal protection of various sub-systems housed inside it is required to have a clear understanding of heat transfer phenomenon due to kinetic heating throughout its trajectory. Typical

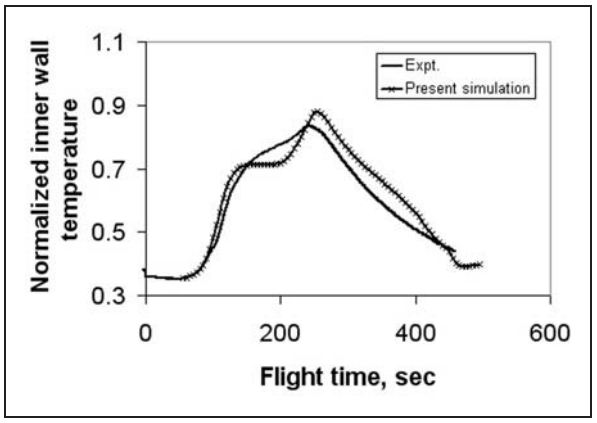

Figure 15. Comparison of normalized inner wall temperature with flight measurements, $X = 480$ mm.

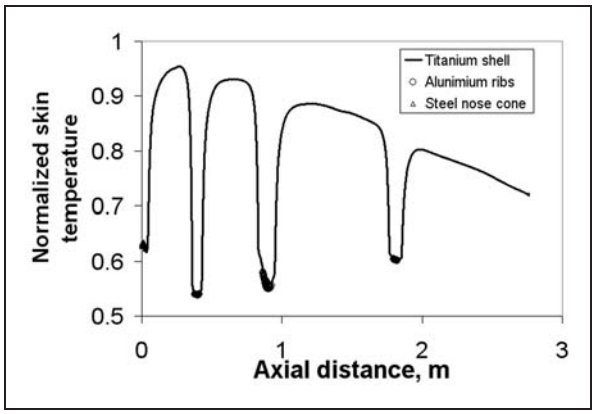

Figure 16. Normalized skin temperature distribution along the vehicle surface, at 256 s.

Mach number and kinetic heating load history of the vehicle is shown in Figure 13. The peak Mach number, stagnation pressure and stagnation temperature are 4.59, 1200 K and 7.2 bar respectively. Indian standard atmospheric model is used to get atmospheric data at different altitudes. The Reynolds Averaged Navier-Stokes equations are solved in air domain and the unsteady heat conduction equation is solved in solid domains. Due to predominant supersonic flow along the trajectory, density based solver is used in the simulation and Menter's SST k-ω[21] is used for modeling turbulence. At the interface between gas-solid and solid-solid, a Flux Forward Temperature Backward (FFTB) method is employed for predicting interface heat flux as well as temperature. Temperature dependent thermodynamic and transport properties (specific heat at constant pressure, viscosity, thermal conductivity etc.) of air[28] and thermophysical properties of structural materials[29] are used in the simulation.

The vehicle nose cone region up to a length of 2.5 m is considered for the computational purposes. The free stream region up to a length of 10 meters from the vehicle surface in radial direction is used in the domain. Structured mesh is generated in the total region including all the solid materials SS-304, titanium shell, aluminum ribs and free stream air. Quadrilateral mesh of size 0.5 million is generated using commercial grid generator as shown in Figure 14. The boundary layer region is resolved by integrating conservative equations right upto the wall without using wall functions. The minimum grid spacing near the missile surface is 10 μm, to achieve y^+ values of the order 1. The predicted normalized skin temperature history at 480 mm from the vehicle nose is compared with the flight measured values in Figure 15. The temperature is normalized with the maximum stagnation temperature. Although, a good overall match is observed, computed skin temperature is lower than the flight measured values in the time between 100 sec to 200 sec and slightly more than the flight measurement afterwards. However, the maximum difference of temperature between the prediction and flight measurement is within 50 K. It is to be mentioned that the vehicle experiences angle of attack up to 12° in its flight, which has not been considered in the present simulation. The normalized skin temperature along the missile surface in longitudinal direction at flight time of 256 s is shown in Figure 16. In general, thermal load will be maximum at stagnation point and decreases along the missile in downstream direction. This phenomenon is clearly observed in the figure. In the titanium sections excluding the adjoining (with other metals) regions, the one dimensional heat conduction is predominant, while near the dissimilar metal junction regions two dimensional heat conduction is clearly visible. Due to its higher thermal diffusivity, aluminum ribs are extracting heat from surrounding titanium shells. This phenomenon is captured in the simulation.

Concluding remarks

Conjugate heat transfer studies are presented for high speed aerospace vehicles using a commercial CFD software. Navier Stokes equations in the fluid domain and transient heat conduction equations in the solid domain are solved simultaneously to obtain the skin temperature history. The energy balance at the gas-solid and solid-solid interface is done by matching both temperature and heat flux at the interface. Computational methodology is first validated by comparing against experimental results of laminar flow past axisymmetric double cone at Mach 4.57 and turbulent flow over circular cylinder at Mach 6.47. Grid independence of the simulation is demonstrated by comparing the results with two different grids and comparing the results. For laminar test case of Mach 4.57 flow over double cone, the simulation crisply captured the bow shock, the separation shock, reattachment shock, the separated flow region and type V shock–boundary layer interaction is observed. Computed flow field, surface temperature

distribution and surface temperature history match nicely with experimental as well as other numerical results reported in the literature. Temperature dependent material properties are found to have significant effect on the surface temperature prediction. For turbulent test case for Mach 6.47 flow over circular cylinder, the computed surface pressure, cold wall heat flux, and surface temperature compare well with experimental results and other numerical results available in the literature. The validated methodology was then applied to predict the surface temperature of a high speed aerospace vehicle and the computed skin temperature is compared with flight measured values. Although, a good overall match is observed, computed skin temperature is lower than the flight measured values in the time between 100 s and 200 s and slightly more than the flight measurement afterwards. It has been observed that near the dissimilar metal junction regions two dimensional heat conduction is predominant.

Funding

This research received no specific grant from any funding agency in the public, commercial, or not-for-profit sectors.

References

1. Thornton EA and Dechumphai P. Coupled flow, thermal and structural analysis of aerodynamically heated panel. *J Aircraft* 1988; 25: 1052–1054.
2. Manna P and Chakraborty D. Numerical investigation of conjugate heat transfer problems. *J Aerosp Sci Technol* 2004; 56: 166–175.
3. Marineau EC. Schetz JA and Neel RE. Turbulent Navier-Stokes simulations of heat transfer with complex wall temperature variations. AIAA Paper No. 2006-3087. San Francisco, California: AIAA.
4. GASP 4.0 User Manual, AeroSoft, ISBN 09652780-5-0, 2002.
5. Hassan B, Kuntz D and Potter DL. Coupled fluid/thermal prediction of ablating hypersonic vehicles, AIAA Paper No. 98-0168. Reno, NV: AIAA.
6. Shope FL. Conjugate conduction-convection heat transfer with a high-speed boundary layer. *J Thermophys Heat Tran* 1994; 8: 275–283.
7. Engblom W, Fletcher B and Georgiadis N. Validation of conjugate heat transfer capability for water-cooled high-speed flows, AIAA Paper No. 2007-4392. Miami, FL: AIAA.
8. Nelson CC and Power GD. CHSSI project CFD-7: The NPARC alliance flow simulation system, AIAA Paper No. 2001-0594. Reno, NV: AIAA.
9. Georgiadis NJ, Yoder DA, Towne CS, Engblom WA, Bhagwandin VA, Power GD, Lankford DW and Nelson CC. Wind-US code physical modelling improvements to complement hypersonic testing and evaluation, AIAA Paper No. 2009-0193. Orlando, Florida: AIAA.
10. Engblom W, Fletcher B and Georgiadis NJ. Conjugate conduction-convection heat transfer for water cooled high-speed flows, AIAA Paper No. 2008-4653. Hartford, CT: AIAA.
11. Perrell ER, Power GD and Robinson C. A modular conjugate heat transfer capability for the Wind-US CFD code, AIAA Paper No. 2010-0031. Orlando, Florida: AIAA.
12. Ferrero P and D'Ambrosio D. A numerical method for conjugate heat transfer problems in hypersonic flows, AIAA Paper No. 2008-4247. Seattle, Washington: AIAA.
13. Harten A, Engquist B, Osher S and Chakravarthy SR. Uniformly high order accurate essentially non-oscillatory schemes, III. *J Comput Phys* 1987; 71: 231–303.
14. Dechaumphai P, Thornton EA and Wieting AR. Flow-thermal structural study of aerodynamically heated leading edges, AIAA Paper No. 88-2245. Williamsburg, VA: AIAA.
15. Dechaumphai P, Thornton EA and Wieting AR. Flow-thermal structural study of aerodynamically heated leading edges. *J Spacecraft* 1989; 26: 201–209.
16. Wieting AR. Experimental study of shock wave interference heating on a cylindrical leading edge. 1987; Ph.D. Dissertation, Old Dominion University, Norfolk, Virginia: also NASA TM-100484, 1987.
17. Zhao X, Sun Z, Tang L and Zheng G. Coupled flow-thermal-structural analysis of hypersonic aerodynamically heated cylindrical leading edge. *Engineering Applications of Computational Fluid Mechanics* 2011; 5: 170–179.
18. Metacomp Technologies. CFD++ User Manual; Version 8.1: Argoura Hills, CA.
19. Fluent 12.1; Theory Manual: 2009.
20. Liou MS. A sequel to AUSM: AUSM+. *Journal of Computational Physic* 1996; 129: 364–382.
21. Menter FR. Two-equation eddy-viscosity turbulence models for engineering applications. *AIAA Journal* 1994; 32: 1598–1605.
22. Menter FR, Langtry RB, Likki SR, Suzen YB, Huang PG and Volker S. A correlation based transition model using local variables, Part-1: model formulation. Paper No. ASME-GT 2004-53452.
23. Francese A. Numerical and experimental Study of UHTC materials for atmospheric re-entry. Ph.D. Dissertation, Department of Space Science and Engineering, L.G. Napolitano, University of Napoli, Federico II, Napoli, Italy.
24. Edney B. Anomalous heat transfer and pressure distribution on blunt bodies at hypersonic speeds in the presence of an impinging shock, FFA Rep. 115. 1968; Aeronaut. Res. Inst. of Sweden.
25. Zimmermann JW. Thermophysical properties of ZrB2 and ZrB2–SiC ceramics. *J Am Ceramic Soc* 2008; 91: 1551–2916.
26. Chase Jr MW. NIST-JANAF themochemical tables, fourth edition. *J Phys Chem Ref Data Monograph* 1998; 9: 1–1951.
27. http://webbook.nist.gov/cgi/cbook.cgi?ID=C12045646&Units=SI&Mask=2#Thermo-Condensed.
28. Incropera FP and Dewitt DP. Fundamentals of heat and mass transfer, 6th edn. John Wiley & Sons Inc., 2007.
29. National Bureau of Standards (USA). 1955; Circ. 564.
30. Metallic Materials Properties Development and Standardization (MMPDS-02), TN21263DL, Federal Aviation Administration, USA, 2005.